Supporting Information

$Cd_2(IO_3)(PO_4)$ and $Cd_{1.62}Mg_{0.38}(IO_3)(PO_4)$: Metal iodate-phosphates with large SHG responses and wide band gaps

Qian-Qian Chen,[ab] Chun-Li Hu,[a] Li-Jia Yao,[ac] Jin Chen,[ab] Ming-Yang Cao,[ab] Bing-Xuan Li,[a] Jiang-Gao Mao*[a]

a. State Key Laboratory of Structural Chemistry, Fujian Institute of Research on the Structure of Matter, Chinese Academy of Sciences, Fuzhou, 350002, P. R. China
b. University of Chinese Academy of Sciences, Beijing 100039, P. R. China
c. School of Physical Science and Technology, ShanghaiTech University, Shanghai 201210, P. R. China
Email: mjg@fjirsm.ac.cn

Table of Contents

Section S1 Materials and Methods.

Synthesis.

$CdCO_3$ (98%, Sigma-Aldrich), NaH_2PO_4 (99%, Aladdin), I_2O_5 (99.5%, Shanghai Chemical reagents Co. Ltd.), $MgBr_2 \cdot 6H_2O$ (98%, Aladdin) and CF_3COOH (99%, Aladdin) were purchased and used without further purification. Crystals of $Cd_2(IO_3)(PO_4)$ and $Cd_{1.62}Mg_{0.38}(IO_3)(PO_4)$ (**1** and **2**) were grown through the hydrothermal methods. For $Cd_2(IO_3)(PO_4)$ (**1**), the starting materials were $CdCO_3$ (0.2983g, 1.73 mmol), NaH_2PO_4 (0.1795 g, 1.50 mmol), I_2O_5 (0.3487 g, 1.04 mmol), CF_3COOH (0.1 mL) and H_2O (2 mL). For $Cd_{1.62}Mg_{0.38}(IO_3)(PO_4)$ (**2**), the loaded materials were $CdCO_3$ (0.2328g, 1.35 mmol), $MgBr_2 \cdot 6H_2O$ (0.3185 g, 1.09 mmol), NaH_2PO_4 (0.3264 g, 2.72 mmol), I_2O_5 (0.4673 g, 1.40 mmol), CF_3COOH (0.1 mL) and H_2O (2 mL). A mixture of the starting materials was loaded in a 23 mL Teflon-lined autoclave, heated to 230 ℃ for 8 h, held at 230 ℃ for 5 days, and cooled to 30 ℃ at 2 ℃/h. For **1** and **2**, the initial and final pH values were 2.0 and 6.0, respectively. Colorless clubbed crystals of **1** and colorless block crystals of **2** were collected by filtration. The yields were about 50% based on Cd.

Instruments and Methods.

Powder X-ray Diffraction.

Powder X-ray diffraction (XRD) patterns were recorded on a Rigaku MiniFlex II diffractometer with graphite-monochromated Cu Kα radiation in the 2θ range of 10°-70° with a step size of 0.02°.

Energy-dispersive X-ray spectroscope.

Microprobe elemental analyses and the elemental distribution maps were measured on a field-emission scanning electron microscope (FESEM, JSM6700F) equipped with an energy-dispersive X-ray spectroscope (EDS, Oxford INCA).

Thermal Analysis.

Thermogravimetric analysis (TGA) and differential scanning calorimetry (DSC)

were performed with a NETZCH STA 449F3 unit under a N_2 atmosphere, at a heating rate of 10 °C/min.

Optical Measurements.

Infrared (IR) spectra were recorded on a Magna 750 FT-IR spectrometer in the form of KBr pellets in the range from 4000 to 400 cm^{-1}. Ultraviolet-visible-near infrared (UV-vis-NIR) spectra in the range of 200-2000 nm were recorded on a PerkinElmer Lambda 950 UV-vis-NIR spectrophotometer. By using *Kubelka-Munk* function,[1] reflectance spectra were converted into absorption spectra.

Second Harmonic Generation Measurements.

Powder SHG measurements were carried out with Q-switch Nd: YAG laser generating radiations at 1064 nm according to Kurtz and Perry method.[2] Crystalline samples in the particle-size range of 210–300 μm were used for SHG measurements. For the phase matching experiments, crystalline samples of **1** and **2** were sieved into distinct particle-size ranges (45–53, 53–75, 75–105, 105–150, 150–210, and 210–300 μm). Sieved KDP samples in corresponding particle-size ranges were taken as references for SHG measurements under 1064 nm laser radiation.

Laser-Induced Damage Threshold Measurement.

Laser-induced damage threshold (LDT) were measured on the crystalline samples using a Q-switched pulsed laser (wavelength, 1064 nm; pulse duration, 10 ns; beam diameter, 1.1 mm; pulse frequency, 1 Hz). An $AgGaS_2$ (AGS) sample of the same size (150–210 μm) was also measured under the same test conditions as references. The LDT of the samples were determined when the samples turned black under the lasing with a gradually increasing emission energy. Because the diameter of the crystallite is much larger than the incident laser wavelength and each crystallite can behave as a macroscopic bulk material, which is similar to the multiphoton absorption, the measurement method is reasonable.[3]

Single Crystal Structure Determination.

Single-crystal X-ray diffraction data were collected on an Agilent Technologies SuperNova dual-wavelength CCD diffractometer with Mo Kα radiation (λ = 0.71073

Å) at 100 K. Data reduction was performed with CrysAlisPro, and absorption correction based on the multi-scan method was applied.[4] The structures were solved with the ShelXT 2014/5 solution program using Intrinsic Phasing methods and by using Olex 2 as the graphical interface.[5-6] The presence of twinning was considered because that the mean value for $|E^2-1|$ (0.656 for **1** and 0.557 for **2**) is much lower than the expected value of 0.736 for the non-centrosymmetric case.[7] For both compounds, the crystals contain both general and racemic twinning, hence twin law -1 0 0 0 0 1 0 1 0 -4 was applied. After applying the twin law, the model was refined with ShelXL 2018/3 using full matrix least squares minimization on F^2.[8] In $Cd_{1.62}Mg_{0.38}(IO_3)(PO_4)$ (**2**), one atomic site (Cd(2)/Mg(1)) was found to be the mixed occupation of Cd and Mg, and they were refined with equal XYZ and thermal displacement factors, the occupancy factors were refined to be 24.645% and 75.355% for Cd(2) and Mg(1), respectively. All of the atoms were refined anisotropically. The structure was checked for missing symmetry elements using PLATON, and none was found.[9] Crystallographic data and structural refinements of the title compounds are listed in Table S1, and the selected bond distances are listed in Table S2 and Table S3. Since both structures were refined as the four-component twins, the Flack parameters cannot be determined.

Computational Method.

Calculations of electronic structure and optical properties for **1** were performed using CASTEP based on density function theory (DFT).[10-11] Norm-conserving pseudopotential was used to treat the electron-core interactions, and GGA-PBE was chosen as exchange-correlation function.[12-13] **2** has a disordered structure which is infeasible for the theoretical calculations. The following orbital electrons were treated as valence electrons: Cd $4d^{10}5s^2$, I $5s^25p^5$, P $3s^23p^3$, and O $2s^22p^4$. The numbers of plane waves included in the basis sets were determined by a cutoff energy of 750 eV for **1**. Monkhorst-Pack k-point sampling of 2 × 2 × 2 for **1** was used to perform numerical integration of Brillouin zone. During the optical property calculations for **1**, more than 1248 empty bands were applied to ensure the convergence of nonlinear

optical coefficients, respectively.

The calculations of second-order NLO susceptibilities were based on length-gauge formalism within the independent particle approximation.[14, 15] The second-order NLO susceptibility can be expressed as

$\chi abc\ \mathrm{L}(-2\omega;\omega,\omega) = \chi abc\ \mathrm{inter}\ (-2\omega;\omega,\omega) + \chi abc\ \mathrm{intra}(-2\omega;\omega,\omega) + \chi abc\ \mathrm{mod}(-2\omega;\omega,\omega)$

where the subscript L denotes the length gauge, χabc inter, χabc intra and χabc mod give the contributions to χabc Lfrom interband processes, intraband processes, and the modulation of interband terms by intraband terms, respectively.

Table S1. Crystallographic data for $Cd_2(IO_3)(PO_4)$ and $Cd_{1.62}Mg_{0.38}(IO_3)(PO_4)$.

formula	Cd_2IPO_7	$Cd_{1.62}Mg_{0.38}IPO_7$
formula weight	494.67	461.47
crystal system	orthorhombic	orthorhombic
space group	*Fdd*2	*Fdd*2
T (K)	100(2)	100(2)
a (Å)	15.366(2)	15.3319(13)
b (Å)	12.374(2)	12.2073(11)
c (Å)	12.324(2)	12.2169(16)
V (Å^3)	2343.3(6)	2286.5(4)
Z	16	16
λ (Mo-K*a*) (Å)	0.71073	0.71073
D_c (g cm^{-3})	5.609	5.362
μ (mm^{-1})	12.787	11.782
goodness of fit on F^2	1.023	1.034
R_1, wR_2 [I >2σ(I)][a]	0.0362, 0.0786	0.0354, 0.0780
R_1, wR_2 (all data)[a]	0.0391, 0.0812	0.0375, 0.0794

[a]$R_1 = \sum||F_o| - |F_c||/\sum|F_o|$, and $wR_2 = \{\sum w[(F_o)^2 - (F_c)^2]^2/\sum w[(F_o)^2]^2\}^{1/2}$.

Table S2. Selected bond distances (Å), BV and BVS for $Cd_2(IO_3)(PO_4)$.

Bond	**Bond Distance**	**BV**	**BVS**
Cd(1)-O(1) #1	2.288(15)	0.354	2.036
Cd(1)-O(2)	2.297(18)	0.346	
Cd(1)-O(3) #2	2.263(16)	0.379	
Cd(1)-O(4) #3	2.339(18)	0.309	
Cd(1)-O(5) #4	2.325(17)	0.321	
Cd(1)-O(6)	2.476(16)	0.213	
Cd(1)-O(7) #4	2.704(15)	0.115	
Cd(2)-O(3) #5	2.284(17)	0.358	2.243
Cd(2)-O(3)	2.283(17)	0.359	
Cd(2)-O(4) #6	2.288(17)	0.354	
Cd(2)-O(4) #7	2.288(17)	0.354	
Cd(2)-O(7) #8	2.235(16)	0.409	
Cd(2)-O(7) #9	2.235(16)	0.409	
Cd(3)-O(1) #10	2.378(16)	0.278	2.076
Cd(3)-O(1)	2.378(16)	0.278	
Cd(3)-O(2) #9	2.275(17)	0.367	
Cd(3)-O(2) #2	2.275(17)	0.367	
Cd(3)-O(6) #10	2.250(16)	0.393	
Cd(3)-O(6)	2.250(16)	0.393	
P(1)-O(1)	1.551(15)	1.195	4.889
P(1)-O(2)	1.530(17)	1.265	
P(1)-O(3)	1.547(15)	1.208	
P(1)-O(4)	1.543(14)	1.221	
I(1)-O(5)	1.811(13)	1.680	5.046
I(1)-O(6)	1.816(17)	1.658	
I(1)-O(7)	1.805(17)	1.708	

Symmetry transformations used to generate equivalent atoms: #1 x-1/4, -y+7/4, z+1/4; #2 -x+1/4, y-1/4, z-1/4; #3 -x, -y+2, z; #4 x-1/4, -y+5/4, z-1/4; #5 -x+1/2, -y+5/2, z; #6 x+1/4, -y+9/4, z+1/4;

#7 -x+1/4, y+1/4, z+1/4; #8 -x+1/4, y+3/4, z-1/4; #9 x+1/4, -y+7/4, z-1/4; #10 -x+1/2, -y+3/2, z.

Table S3. Selected bond distances (Å), BV and BVS for $Cd_{1.62}Mg_{0.38}(IO_3)(PO_4)$.

Bond	**Bond Distance**	**BV**	**BVS**
Cd(1)-O(1) #1	2.322(14)	0.323	2.044
Cd(1)-O(2)	2.290(17)	0.352	
Cd(1)-O(3) #2	2.291(14)	0.351	
Cd(1)-O(4) #3	2.321(15)	0.324	
Cd(1)-O(5) #4	2.262(16)	0.380	
Cd(1)-O(6)	2.449(14)	0.229	
Cd(1)-O(7) #4	2.822(15)	0.084	
Cd(2)-O(3) #5	2.131(14)	0.541	2.185
Cd(2)-O(3)	2.131(14)	0.541	
Cd(2)-O(4) #6	2.178(15)	0.477	
Cd(2)-O(4) #7	2.178(15)	0.477	
Cd(2)-O(7) #8	2.089(16)	0.607	
Cd(2)-O(7) #9	2.089(16)	0.607	
Mg(1)-O(3)	2.131(14)	0.306	
Mg(1)-O(3) #5	2.131(14)	0.306	
Mg(1)-O(4) #6	2.178(15)	0.270	
Mg(1)-O(4) #7	2.178(15)	0.270	
Mg(1)-O(7) #8	2.089(16)	0.343	
Mg(1)-O(7) #9	2.089(16)	0.343	
Cd(3)-O(1) #10	2.387(17)	0.271	2.090
Cd(3)-O(1)	2.387(17)	0.271	
Cd(3)-O(2) #8	2.291(16)	0.351	
Cd(3)-O(2) #2	2.291(16)	0.351	
Cd(3)-O(6)	2.223(14)	0.422	
Cd(3)-O(6) #10	2.222(14)	0.423	
P(1)-O(1)	1.551(14)	1.195	5.047
P(1)-O(2)	1.520(15)	1.300	

P(1)-O(3)	1.538(13)	1.238	
P(1)-O(4)	1.516(13)	1.314	
I(1)-O(5)	1.824(12)	1.622	4.908
I(1)-O(6)	1.806(16)	1.703	
I(1)-O(7)	1.833(15)	1.583	

Symmetry transformations used to generate equivalent atoms: #1 x+1/4, -y+7/4, z -1/4; #2 -x+3/4, y-1/4, z+1/4; #3 -x+1, -y+2, z; #4 x+1/4, -y+5/4, z+1/4; #5 -x+1/2, -y+5/2, z; #6 -x+3/4, y+1/4, z-1/4; #7 x-1/4, -y+9/4, z-1/4; #8 x-1/4, -y+7/4, z+1/4; #9 -x+3/4, y+3/4, z+1/4; #10 -x+1/2, -y+3/2, z.

Table S4. The assignments of the infrared absorption peaks for $Cd_2(IO_3)(PO_4)$ and $Cd_{1.62}Mg_{0.38}(IO_3)(PO_4)$.

Mode description (cm^{-1})	$Cd_2(IO_3)(PO_4)$	$Cd_{1.62}Mg_{0.38}(IO_3)(PO_4)$
P-O vibrations	1047, 974	1050, 979
I-O vibrations	794, 735	796, 747
Cd-O vibrations	591, 574, 548, 433	592, 578, 554, 428

Table S5. Calculated dipole moments for CdO_n (n=6, 7), $I(1)O_3$, $P(1)O_4$ and net dipole moment for a unit cell in $Cd_2(IO_3)(PO_4)$.

$Cd_2(IO_3)(PO_4)$ (Z=16)				
Polar unit	Dipole moment (D = Debyes)			
	total magnitude	x-component	y-component	z-component
$Cd(1)O_7$	0.46	(±0.04)×8	(±0.21)×8	(-0.41)×16
$Cd(2)O_6$	0.13	0×8	$(\pm 7.55\times10^{-15})\times4$	(0.13)×8
$Cd(3)O_6$	1.86	$(\pm 7.11\times10^{-15})\times4$	0×8	(-1.86)×8
$I(1)O_3$	16.20	(±6.24)×8	(±10.99)×8	(-10.13)×16
$P(1)O_4$	0.55	(±0.11)×8	(±0.35)×8	(-0.41)×16
Net dipole moment (a unit cell)	189.04	0	0	-189.04

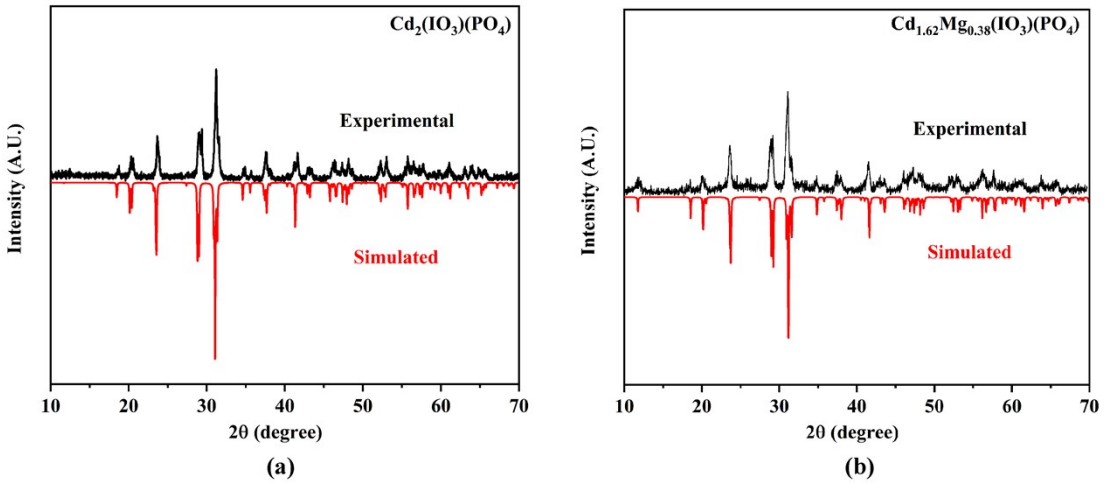

Figure S1. Simulated and experimental powder X-ray diffraction patterns of $Cd_2(IO_3)(PO_4)$ (a) and $Cd_{1.62}Mg_{0.38}(IO_3)(PO_4)$ (b).

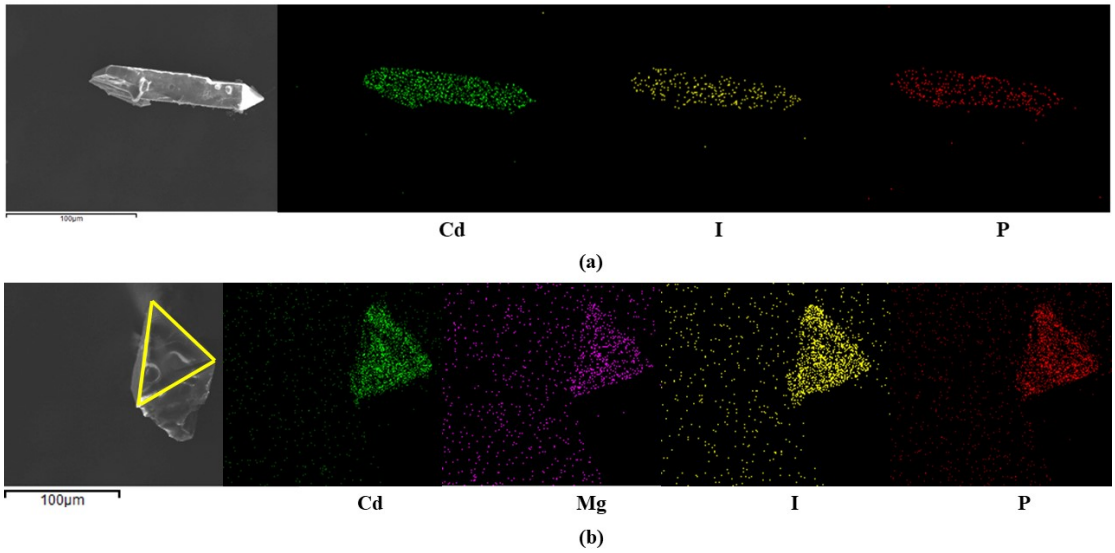

Figure S2. SEM images and their elemental distribution maps of $Cd_2(IO_3)(PO_4)$ (a) and $Cd_{1.62}Mg_{0.38}(IO_3)(PO_4)$ (b).

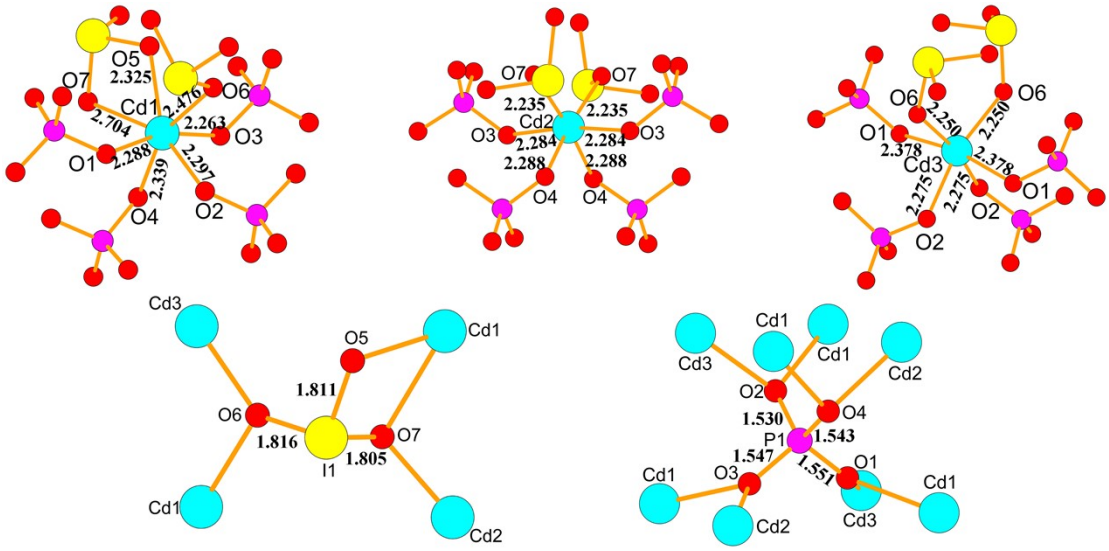

Figure S3. The connectivity modes of the IO_3, PO_4 groups and Cd^{2+} ions in $Cd_2(IO_3)(PO_4)$.

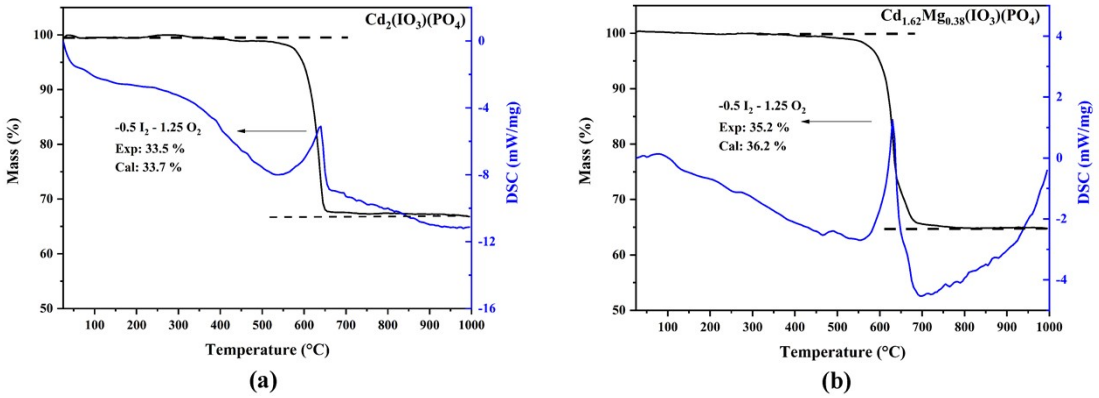

Figure S4. TGA and DSC curves of $Cd_2(IO_3)(PO_4)$ (a) and $Cd_{1.62}Mg_{0.38}(IO_3)(PO_4)$ (b) under a N_2 atmosphere.

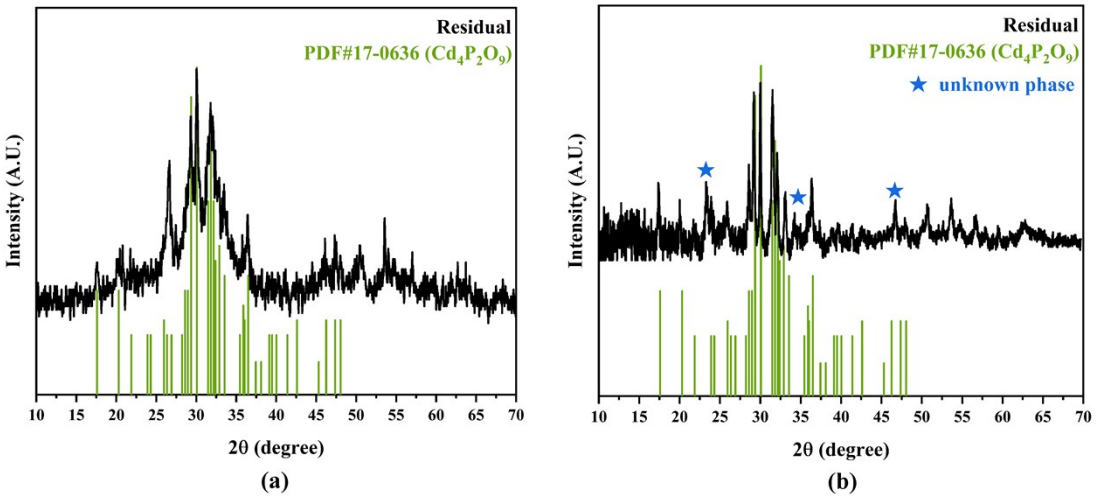

Figure S5. The powder X-ray diffraction patterns of the residuals under 1000 ℃ of $Cd_2(IO_3)(PO_4)$ (a) and $Cd_{1.62}Mg_{0.38}(IO_3)(PO_4)$ (b).

According to the Figure S5(a), the residual of $Cd_2(IO_3)(PO_4)$ is $Cd_4P_2O_9$. (PDF#17-0636 only marks peaks at 2θ =15-50°.)[16] According to the residual and the weight loss of Figure S4(a), $Cd_2(IO_3)(PO_4)$ lost 0.5 I_2 and 1.25 O_2 per formula unit in the thermogravimetric process. According to the Figure S5(b), most of the residual of $Cd_{1.62}Mg_{0.38}(IO_3)(PO_4)$ is $Cd_4P_2O_9$, and there are some peaks that have not been assigned via suitable PDF cards. EDS analysis showed that the residual of $Cd_{1.62}Mg_{0.38}(IO_3)(PO_4)$ contained Cd, Mg, P and O. According to the weight loss of Figure S4(b), $Cd_{1.62}Mg_{0.38}(IO_3)(PO_4)$ lost 0.5 I_2 and 1.25 O_2 per formula unit in the thermogravimetric process.

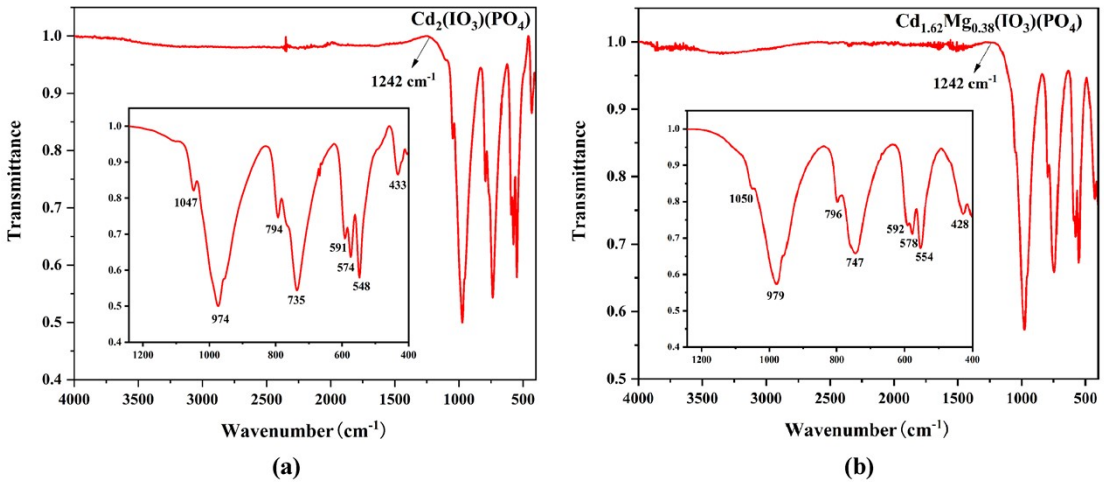

Figure S6. IR spectra for $Cd_2(IO_3)(PO_4)$ (a) and $Cd_{1.62}Mg_{0.38}(IO_3)(PO_4)$ (b).

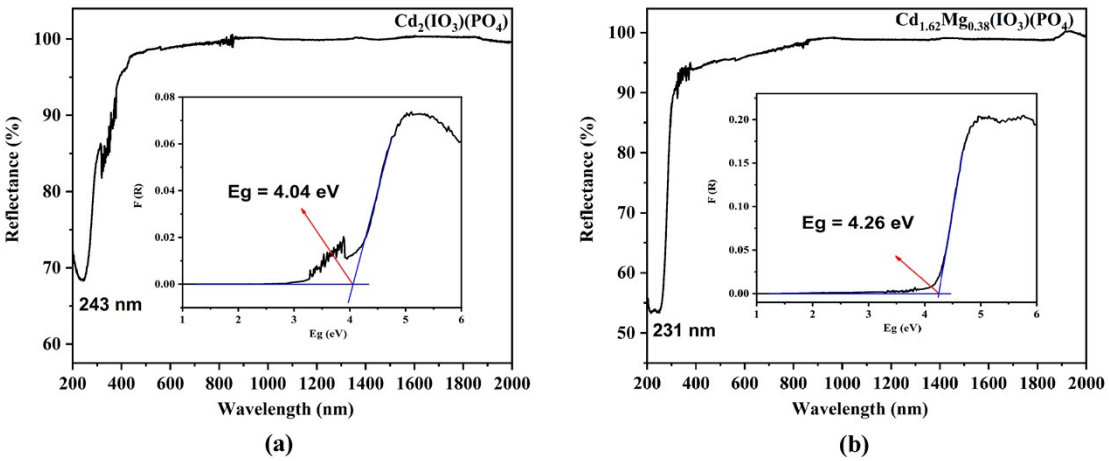

Figure S7. UV-vis-IR spectra of $Cd_2(IO_3)(PO_4)$ (a) and $Cd_{1.62}Mg_{0.38}(IO_3)(PO_4)$ (b).

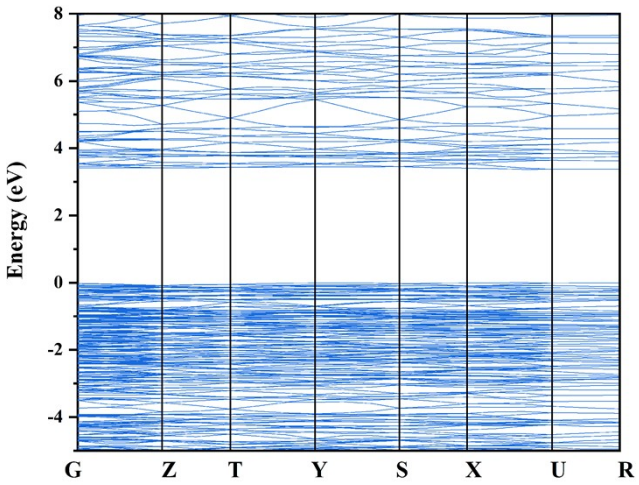

Figure S8. The calculated band structure of $Cd_2(IO_3)(PO_4)$.

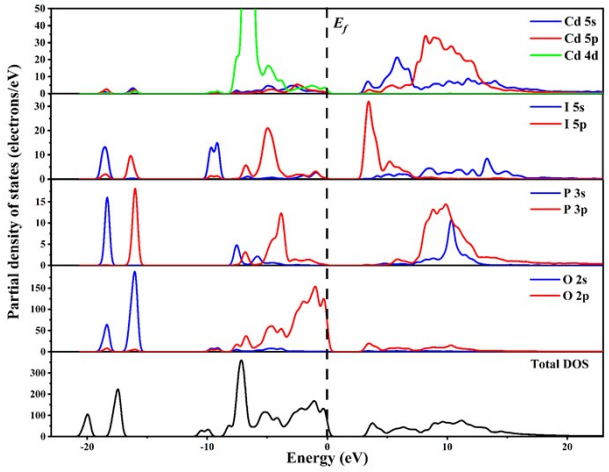

Figure S9. The partial and total density of states for $Cd_2(IO_3)(PO_4)$.

References

1. P. Kubelka and F. Munk, *Z. Tech. Physical*, 1931, **12**, 886-892.
2. S. K. Kutz and T. T. Perry, *J. Appl. Phys.*, 1968, **39**, 3798-3813.
3. M. J. Zhang, B. X. Li, B. W. Liu, Y. H. Fan, X. G. Li, H. Y. Zeng and G. C Guo, *Dalton Trans.*, 2013, **42**, 14223-14229.
4. R. H. Blessing, *Acta Crystallogr. Sect. A*, 1995, **51**, 33-38.
5. G. M. Sheldrick, *Acta Crystallogr. Sect. A*, 2015, **71**, 3-8.
6. O. V. Dolomanov, L. J. Bourhis, R. J. Gildea, J. A. K. Howard and H. Puschmann, *J. Appl. Crystallogr.*, 2009, **42**, 339-341.
7. R. Herbst-Irmer and G. M. Sheldrick, *Acta Crystallogr. Sect. B*, 1998, **54**, 443-449.
8. G. M. Sheldrick, *Acta Crystallogr. Sect. C*, 2015, **71**, 3-8.
9. A. L. Spek, *J. Appl. Crystallogr.*, 2003, **36**, 7-13.
10. M. D. Segall, P. J. D. Lindan, M. J. Probert, C. J. Pickard, P. J. Hasnip, S. J. Clark and M. C. Payne, *J. Phys.: Condens. Mat.*, 2002, **14**, 2717-2744.
11. V. Milman, B. Winkler, J. A. White, C. J. Pickard, M. C. Payne, E. V. Akhmatskaya and R. H. Nobes, *Int. J. Quantum Chem.*, 2000, **77**, 895-910.
12. J. P. Perdew, K. Burke and M. Ernzerhof, *Phys. Rev. Lett.*, 1996, **77**, 3865-3868.
13. J. S. Lin, A. Qteish, M. C. Payne and V. Heine, *Phys Rev B*, 1993, **47**, 4174-4180.
14. J. E. Sipe and Ed Ghahramani, *Phys. Rev. B*, 1993, **48**, 11705-11722.
15. S. Sharma, J. K. Dewhurst and C. Ambrosch-Draxl, *Phys. Rev. B*, 2003, **67**, 165332.
16. J. J. Brown and F. A. Hummel, *J. Electrochem. Soc.*, 1964, **111**, 1052-1057.